Cell Reports
Article

Cell PRESS
Open ACCESS

NLRP3 Inflammasome Blockade Inhibits VEGF-A-Induced Age-Related Macular Degeneration

Alexander G. Marneros[1,2,*]
[1]Cutaneous Biology Research Center, Massachusetts General Hospital, Charlestown, MA 02129, USA
[2]Department of Dermatology, Harvard Medical School, Charlestown, MA 02129, USA
*Correspondence: amarneros@partners.org
http://dx.doi.org/10.1016/j.celrep.2013.08.002
This is an open-access article distributed under the terms of the Creative Commons Attribution-NonCommercial-No Derivative Works License, which permits non-commercial use, distribution, and reproduction in any medium, provided the original author and source are credited.

SUMMARY

The NLRP3 inflammasome is activated in age-related macular degeneration (AMD), but it remains unknown whether its activation contributes to AMD pathologies. VEGF-A is increased in neovascular ("wet") AMD, but it is not known whether it plays a role in inflammasome activation, whether an increase of VEGF-A by itself is sufficient to cause neovascular AMD and whether it can contribute to nonexudative ("dry") AMD that often co-occurs with the neovascular form. Here, it is shown that an increase in VEGF-A results in NLRP3 inflammasome activation and is sufficient to cause both forms of AMD pathologies. Targeting NLRP3 or the inflammasome effector cytokine IL-1β inhibits but does not prevent VEGF-A-induced AMD pathologies, whereas targeting IL-18 promotes AMD. Thus, increased VEGF-A provides a unifying pathomechanism for both forms of AMD; combining therapeutic inhibition of both VEGF-A and IL-1β or the NLRP3 inflammasome is therefore likely to suppress both forms of AMD.

INTRODUCTION

Age-related macular degeneration (AMD) is the most common cause of irreversible blindness in the elderly (Friedman et al., 2004; van Leeuwen et al., 2003). AMD manifests with the cardinal features of progressive atrophic degeneration of the retinal pigment epithelium (RPE) with sub-RPE deposits that affect metabolic exchanges between the RPE and choroidal vessels in nonexudative ("dry") AMD or with choroidal neovascularization (CNV) in neovascular ("wet") AMD (Bird et al., 1995; Kliffen et al., 1997). Importantly, patients with nonexudative AMD can progress to develop neovascular AMD, and both forms of AMD can occur simultaneously, suggesting a common pathomechanism that is currently unknown, in part due to the lack of a mouse model with features of both forms of AMD (Sunness et al., 1999).

Increased VEGF-A levels have been observed in neovascular AMD, but it remains to be shown whether an increase in VEGF-A alone is sufficient to cause neovascular AMD and through which pathomechanisms it may promote the disease process (Funk et al., 2009). Increased hypoxia and oxidative damage to the RPE have been regarded as critical factors in AMD pathogenesis, which induce VEGF-A expression in the RPE (Klettner and Roider, 2009). Consistent with the observed increased VEGF-A levels in neovascular AMD, anti-VEGF-A treatments have shown significant clinical benefit in patients with neovascular AMD (Martin et al., 2011). In contrast, nonexudative AMD is more common than neovascular AMD and causes loss of vision in millions of individuals, but no established treatments exist for nonexudative AMD. Thus, identifying a common pathogenetic step for both forms of AMD would provide the opportunity for a targeted broad therapeutic approach for neovascular and nonexudative AMD.

Genetic association data have provided evidence for linkage of both forms of advanced AMD with the VEGF-A gene locus (Fritsche et al., 2013; Yu et al., 2011), suggesting that increased VEGF-A levels may promote not only neovascular AMD but also nonexudative AMD. Thus, both forms of AMD may arise as distinct manifestations of a common underlying process of VEGF-A dysregulation.

Recently, NLRP3 inflammasome activation has been reported in both nonexudative and neovascular AMD, but it is not known whether VEGF-A promotes its activation (Kaneko et al., 2011; Tarallo et al., 2012; Tseng et al., 2013). Activation of the NLRP3 inflammasome results in autocatalytic cleavage of caspase-1 precursor (with the generation of the active p10 and p20 subunits), which leads to proteolytic activation of the potent proinflammatory cytokines IL-1β and IL-18 (Latz et al., 2013). Importantly, inflammasome activation has been suggested to influence various metabolic and aging diseases, including atherosclerosis, diabetes, gout, or obesity (Wen et al., 2012). However, it is not known whether NLRP3 inflammasome activation has a pathogenic role in the development of AMD, due to the lack of a mouse model that manifests chorioretinal pathologies as seen in both forms of AMD with progressive age, in which the role of the inflammasome could be tested. Recent studies have proposed either an inhibitory or a promoting role of the NLRP3 inflammasome for AMD (Doyle et al., 2012; Tarallo et al., 2012). Inhibition of the NLRP3 inflammasome prevented RPE degeneration, induced by DICER1 loss or *Alu* RNA exposure, whereas it increased neovascular lesions in an acute laser wound-healing model (Doyle et al., 2012; Tarallo et al., 2012).

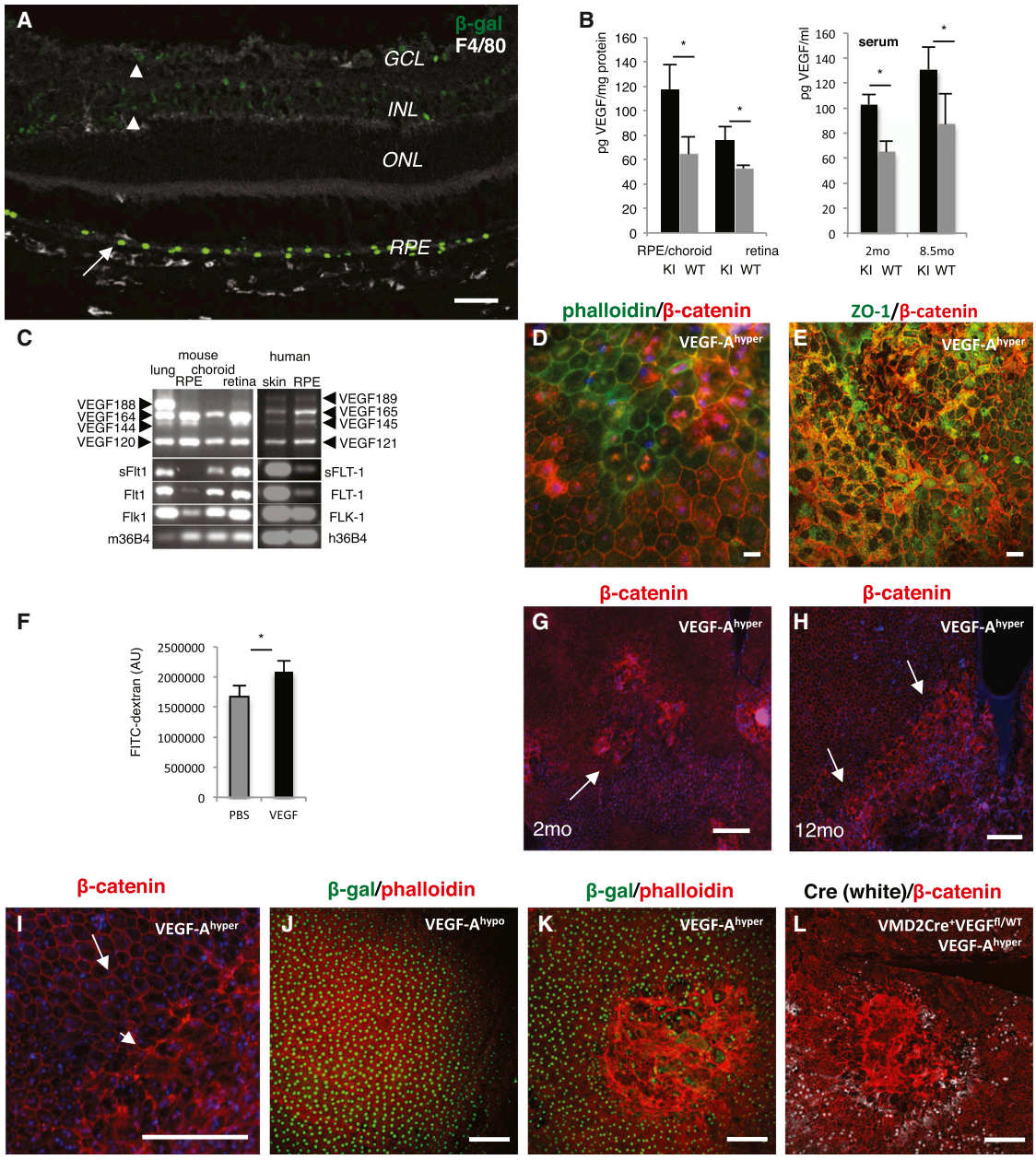

Figure 1. Increased VEGF-A Levels Result in a Progressive RPE Barrier Breakdown

(A) The RPE is the main cell type of VEGF-A expression in the adult eye. Immunolabeling of an adult posterior eye of a VEGF-A^{hyper} mouse (15 months old) for β-gal reflects cellular expression of VEGF-A (green). Strong VEGF-A expression is observed in RPE cells (arrow), whereas low-level VEGF-A expression is seen in retinal cells of the ganglion cell layer (GCL) and inner nuclear layer (INL) (arrowheads), but not the photoreceptor layer (ONL). Scale bar, 50 μm.

(B) VEGF-A ELISA of RPE/choroid and retinal tissue in adult VEGF-A^{hyper} mice (KI) and control littermate (WT) mice (n = 7/group) shows a significant increase of VEGF-A levels in the RPE/choroid tissues in VEGF-A^{hyper} mice. Serum levels of VEGF-A are elevated in mutant mice independently of age as well (n = 3/group). Error bars, mean ± SD. *$p < 0.05$.

(C) Mouse and human RPE cells express the VEGF-A receptors Flt1 and Flk1 and all major VEGF-A isoforms, particularly VEGF-A^{164} and VEGF-A^{120} (VEGF-A^{165} and VEGF-A^{121} in human).

(D) Focal RPE barrier breakdown is observed in VEGF-A^{hyper} mice with cytoplasmic and nuclear accumulation of β-catenin. Colabeling with Alexa 488-conjugated phalloidin (green) shows that in normal RPE cells, phalloidin and β-catenin (red) labeling is strongest along cell membranes, whereas in RPE cells with RPE barrier breakdown, β-catenin labeling along the cell membranes is attenuated and increased in the nuclei or cytoplasm. A 7-month-old VEGF-A^{hyper} mouse is shown. Scale bar, 20 μm.

(E) Colabeling of cell junction proteins β-catenin (red) and ZO-1 (green) shows loss of membrane-bound ZO-1 and β-catenin with nuclear and cytoplasmic accumulation. A 7-month-old VEGF-A^{hyper} mouse is shown. Scale bar, 50 μm.

(legend continued on next page)

However, these studies were limited by the use of experimental models that do not reflect the age-dependent progressive chorioretinal pathologies seen in AMD, such as the acute laser injury model in which neovascularization occurs in the setting of healthy RPE cells, which is in fact an acute wound-healing model and only a very limited model for neovascular AMD (He and Marneros, 2013). Thus, the role of the NLRP3 inflammasome in such an acute wound-healing model is likely to differ from its role in human AMD or in a mouse model that develops cardinal features of AMD in a progressive age-dependent manner accompanied by degenerative RPE changes.

Here, mice with increased VEGF-A levels are shown to develop age-dependent progressive cardinal features of both nonexudative and neovascular AMD, in which NLRP3 inflammasome activation occurs as seen in human AMD. Targeting NLRP3 or the inflammasome effector cytokine IL-1β reduces VEGF-A-induced chorioretinal pathologies in these mice, such as RPE barrier breakdown and CNV lesions, whereas IL-18 deficiency promotes CNV lesions. The data provide a unifying pathomechanism for both forms of AMD and show that what has been considered as a multifactorial pathogenesis can be triggered by an increase of a single growth factor, VEGF-A, which induces NLRP3 inflammasome activation to promote AMD-like pathologies.

RESULTS

Age-Dependent RPE Barrier Breakdown in Mice with Increased VEGF-A Levels

To determine whether an increase in VEGF-A by itself is sufficient to cause eye pathologies as seen in AMD, mutant mice were analyzed that have increased VEGF-A protein levels. The increase of VEGF-A levels occurs in adult heterozygote VEGF-$A^{lacZKI/WT}$ mice (hereafter described as VEGF-A^{hyper} mice) as a consequence of the insertion of an IRES-NLS-lacZ-SV40pA sequence into the 3′ UTR of the VEGF-A gene locus at +202 bp 3′ to the stop codon (Cervi et al., 2007; Miquerol et al., 1999), which removes miRNA binding sites in the 3′ UTR that would inhibit VEGF-A mRNA translation (Jafarifar et al., 2011). Adult transgenic mice that express lacZ driven by a promoter that is active in RPE cells (Dct-lacZ-SV40pA mice) (Wilkie et al., 2002) showed no eye abnormalities, suggesting that changes observed in the eyes of VEGF-A^{hyper} mice are due to increased VEGF-A levels, and not due to the insertion of the lacZ sequence and β-galactosidase (β-gal) expression in RPE cells. In additional control experiments, mice were examined in which the IRES-NLS-lacZ-SV40pA sequence was inserted immediately after the VEGF-A stop codon, resulting in a hypomorphic VEGF-A allele (VEGF-A^{hypo} mice) while maintaining β-gal expression from the endogenous VEGF-A locus (Damert et al., 2002). These VEGF-A^{hypo} mice showed β-gal expression in ocular tissues like VEGF-A^{hyper} mice, but without ocular pathologies, further demonstrating that the observed eye changes in VEGF-A^{hyper} mice are due to the increased VEGF-A levels (Figures 1J and 1K).

In these VEGF-A^{hyper} mice, nuclear β-gal expression (due to the nuclear localization signal between the IRES sequence and the lacZ) reflects accurately VEGF-A expression at single-cell resolution (Figures 1A, S1A, and S1B). The use of an IRES sequence allows independent translation of both VEGF-A and the lacZ reporter from the same bicistronic mRNA produced by the targeted allele. Choroid/RPE tissues as well as retinas from adult VEGF-A^{hyper} mice showed significantly increased VEGF-A protein levels compared to control littermate mice, albeit retinas having lower VEGF-A levels (Figure 1B). Consistent with this observation, staining for β-gal showed that RPE cells are the main cell type in the choroid and retina to express VEGF-A and that strong VEGF-A expression in the RPE is maintained at all ages (up to 24-month-old mice were studied) (Figure 1A). Similarly, VEGF-A serum levels were increased in VEGF-A^{hyper} mice, and this increase was maintained with progressive age (Figure 1B). A cell line derived from human RPE cells, ARPE-19 cells, and freshly isolated primary mouse RPE cells express the VEGF-A receptors Flt1 and Flk1, and all major VEGF-A isoforms, most prominently VEGF-A^{164} and VEGF-A^{120} (VEGF-A^{165} and VEGF-A^{121} in human) (Figure 1C). VEGF-A treatment of ARPE-19 cells induced phosphorylation of VEGFR2 and its downstream target AKT, which could be blocked by a specific VEGFR2 kinase inhibitor (Figure S1C), demonstrating that VEGF-A can elicit VEGFR2-dependent VEGF-A pathway activation in RPE cells.

VEGF-A pathway activation can lead to RPE barrier breakdown of RPE monolayers in vitro (Ablonczy et al., 2011). To test whether increased VEGF-A levels in VEGF-A^{hyper} mice are associated with RPE barrier disruption, choroidal flat mounts from these mice were stained for β-catenin and zonula

(F) FITC-dextran flux assays with RPE cells demonstrate that VEGF-A^{165} treatment induces barrier breakdown and increased transepithelial flux of 10 kDa FITC-dextran (n = 3). Error bars, mean ± SD. *p < 0.05. y axis indicates fluorescence arbitrary units (AU).
(G and H) Choroidal flat mount staining of eyes from VEGF-A^{hyper} mice with β-catenin (red) shows that RPE barrier breakdown is observed in small foci (arrow) in young VEGF-A^{hyper} eyes (2 months old; G) but that these areas expand and become confluent and affect most of the posterior eye (arrows) with progressive age of the mice (12 months old; H). Scale bars, 200 μm.
(I) Magnification of area from (H) that delineates normal-appearing RPE (arrow) with its honeycomb pattern from lesional abnormal-appearing RPE cells (arrowhead). Scale bar, 200 μm.
(J) Adult VEGF-A^{hypo} mice, hypomorphic for VEGF-A, express β-gal (green) from the endogenous VEGF-A gene locus but show normal RPE cells. Scale bar, 100 μm.
(K) In contrast, adult VEGF-A^{hyper} mice, with increased VEGF-A levels, show the same expression of β-gal (green) from the endogenous VEGF-A gene locus as VEGF-A^{hypo} mice but show multifocal RPE barrier breakdown. Scale bar, 100 μm.
(L) Mice that express VMD2-Cre specifically in RPE cells (white nuclear staining for Cre) that are heterozygous for VEGF-$A^{fl/fl}$ and carry the VEGF-A^{hyper} allele; in these mice, Cre^{+} RPE cells are expected to have lower levels of VEGF-A than Cre^{-} RPE cells. RPE barrier breakdown occurs predominantly within Cre^{-} RPE patches, therefore expressing higher levels of VEGF-A. Scale bar, 100 μm.
See also Figure S1.

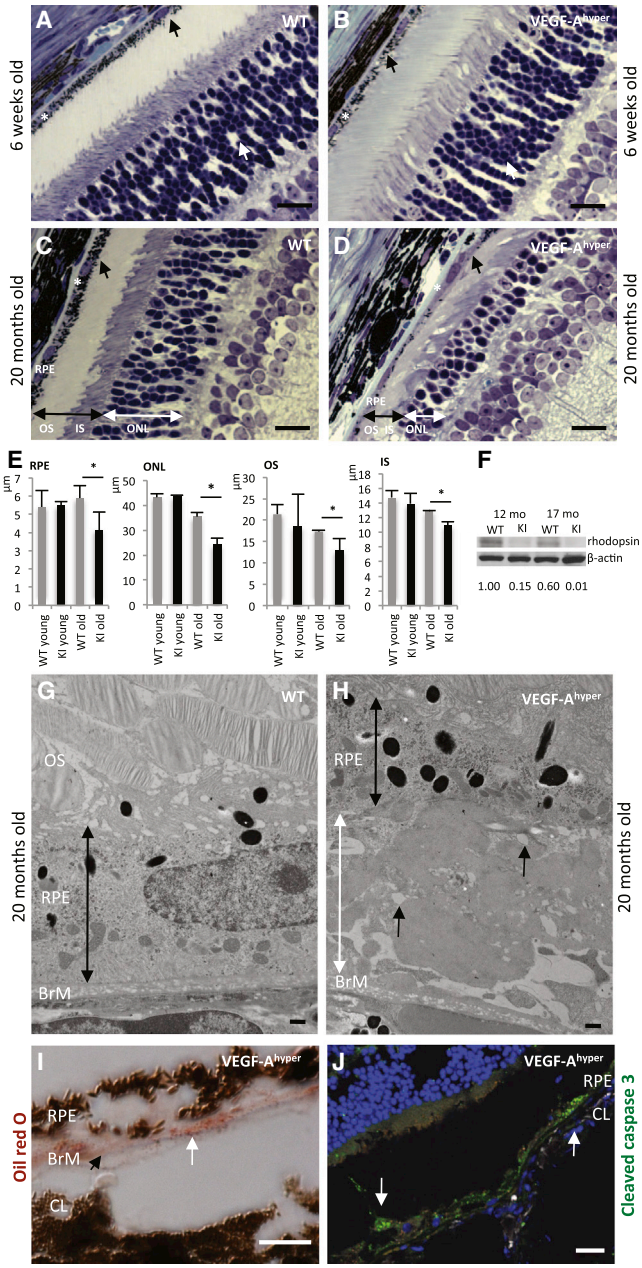

Figure 2. Progressive Age-Dependent Degeneration of the RPE and Photoreceptors in Mice with Increased VEGF-A Levels

(A–D) Although the retina and choroid/RPE appear unremarkable in young adult VEGF-A^{hyper} mice (6 weeks old; B), with progressive age, a severe RPE atrophy is noticed with loss of pigment granules, thinning of RPE cells, and massive sub-RPE deposit accumulation (black arrow in D). The photoreceptor nuclear layer (ONL) is severely attenuated (white double arrow in D) compared to age-matched littermate control retinas (C). In addition, photoreceptor inner and outer segments (black double arrow) are significantly shortened (D). Scale bars, 20 µm. The asterisks (*) indicate Bruch's membrane.

(E) Quantification of RPE and photoreceptor length reveals significantly thinned RPE and attenuated photoreceptor outer and inner segments (OS and IS, respectively) and ONL in aged mutant mice (20 months of age). n = 5/group. Error bars, mean ± SD. *$p < 0.05$.

(F) Photoreceptor degeneration is reflected in reduced rhodopsin protein levels in posterior eyes of aged VEGF-A^{hyper} mice (KI, 12 and 17 months old) compared to control littermate mice (WT). Normalized densitometric values are indicated.

(G and H) Electron microscopy demonstrates massive accumulation of basal laminar sub-RPE deposits in aged (20 months old; H) VEGF-A^{hyper} mice compared to age-matched control littermate mice (G). The RPE is thinned in VEGF-A^{hyper} mice (black double arrow), sub-RPE deposits (white double arrow) consist of electron-dense deposits resembling basal laminar deposits, and electron-lucent spaces indicate lipid-like material that was removed during fixation (black arrows). BrM, Bruch's membrane. OS, photoreceptor outer segments. Scale bars, 500 nm.

(I) Oil red O staining in an aged VEGF-A^{hyper} mouse shows accumulation of lipid droplets in sub-RPE deposits (white arrow). Black arrowhead points to Bruch's membrane. CL, choroidal layer. Scale bar, 10 µm.

(J) RPE cell degeneration in aged VEGF-A^{hyper} mice (15 months old) with RPE cells focally undergoing cell death, demonstrated by cleaved caspase-3 (Asp175) immunostaining (white arrows). Scale bar, 50 µm.

See also Figure S2.

occludens-1 (ZO-1). In RPE cells of young VEGF-A^{hyper} mice and in healthy control mice, immunolabeling for β-catenin and ZO-1 shows a membrane-bound localization, as β-catenin is part of the adherens junctions, and ZO-1 is part of the tight junctions, both comprising the RPE barrier. In adult VEGF-A^{hyper} mice, focal RPE cytoskeletal abnormalities were observed with loss of the typical RPE honeycomb cell morphology, and these changes were associated with loss of membrane-bound ZO-1 and β-catenin and their increased cytoplasmic and nuclear accumulation, providing a morphologic correlate to RPE barrier breakdown (Figures 1D and 1E). These changes were observed in all VEGF-A^{hyper} mice examined, whereas they were not seen in any control littermate mice (>200 mutant and control mice were examined between the ages of 4 weeks and 24 months of age).

Although young VEGF-A^{hyper} mice showed multiple small foci of RPE barrier breakdown and morphological abnormalities of the RPE (Figure 1G), aged mice (>7 months old) showed large confluent areas of these defects, mostly in the central part of the posterior eye (Figures 1H and 1I). Thus, a chronic increase of VEGF-A levels is sufficient to cause an age-dependent progressive RPE barrier breakdown in vivo. Furthermore, VEGF-A treatment of human RPE monolayers resulted in a rapid breakdown of barrier function in FITC-dextran flux assays (Figure 1F), suggesting that the observed RPE barrier breakdown in VEGF-A^{hyper} mice is a direct consequence of increased VEGF-A levels. To provide further evidence for a direct role of VEGF-A for RPE barrier breakdown in vivo, mice were generated that become heterozygous for VEGF-A postnatally, specifically in patches of the RPE, and carry the VEGF-A^{hyper} allele (VMD2-Cre^{+}VEGF-A$^{fl/WT}$VEGF-A^{hyper} mice). In these mice, foci of RPE barrier breakdown were observed primarily at areas of the RPE with absence of Cre expression (and thus increased VEGF-A levels), and not in Cre-positive RPE patches (with normalized VEGF-A levels) (Figure 1L).

Increased VEGF-A Levels Are Associated with Cardinal Features of Nonexudative AMD

Eyes from VEGF-A^{hyper} mice and control mice were examined up to 24 months of age, revealing an age-dependent progressive RPE atrophy and degenerative changes with loss of RPE pigment granules in mutant mice (Figures 2D, S2C, and S2G).

Although young mutant mice have a normal morphological appearance of most of the RPE and retina (Figure 2B), older mice showed progressive degeneration of the RPE, with some RPE cells undergoing cell death with positive staining for cleaved caspase-3 (Asp175) (Figure 2J). The RPE defects were associated with severe progressive age-dependent degeneration of the photoreceptors, with shortening of the photoreceptor outer and inner segments and a significant attenuation of the photoreceptor nuclear cell layer (outer nuclear layer [ONL]) (Figures 2D, 2E, S2G, and S2H). Apoptotic nuclei of photoreceptors were also observed, and rhodopsin levels were significantly reduced in retinas of aged VEGF-A^{hyper} mice (Figures 2F, S2G, and S3G), reflecting photoreceptor degeneration. Electron microscopy revealed massive age-dependent electron-dense sub-RPE deposit formation (Figures 2H, S2B, and S2E), strongly resembling basal laminar deposits in AMD. Droplet-like electron-lucent spaces within these deposits (Figures 2H, S2C, and S2D) indicate lipid accumulation removed during fixation, as has been reported in basal laminar deposits in human AMD (Curcio et al., 2005b), further supported by oil red O-positive sub-RPE accumulations (Figure 2I). Furthermore, "wide-spaced collagen"-like material could be seen in these sub-RPE deposits (Figure S2B), a typical finding in human AMD. These deposits were not observed in young VEGF-A^{hyper} mice, whereas sub-RPE deposits increased progressively with age. Vacuolar degeneration of RPE cells (Figures S2E and S2F), also found in human eyes with early AMD (Anderson et al., 2002), was an early sign of RPE damage and could already be seen focally in the eyes of young VEGF-A^{hyper} mice, before the onset of photoreceptor loss (Figures 5A and S3C). In addition, round phalloidin-negative autofluorescent droplet-like sub-RPE deposits accumulated with progressive age particularly at sites where RPE cells had lost their normal honeycomb pattern morphology (Figures S2I, S2J, and 4D–4G; these deposits where also negative for F4/80 as seen in Figure S3E).

Thus, a chronic increase of VEGF-A levels leads to early degenerative changes in the RPE and progressive basal laminar sub-RPE deposit formation with subsequent degeneration of photoreceptors. Choroidal vessels maintained endothelial fenestrations, and perfusion experiments with fluorescein-labeled lectins did not show a significant abnormality in choroidal perfusion, suggesting that the RPE degeneration is not a consequence of a choroidal vascular perfusion defect (Figure 3A).

Progressive CNV as in Neovascular AMD in VEGF-A^{hyper} Mice

Disruption of the RPE barrier would be expected to lead to degeneration of photoreceptors and accumulation of a subretinal inflammatory cell infiltrate. Indeed, at sites of RPE barrier breakdown, increased photoreceptor apoptosis was seen in VEGF-A^{hyper} mice (Figure S3G), as well as a subretinal myeloid cell inflammatory infiltrate (Figures S3E and S3H).

It has been hypothesized that RPE barrier breakdown and a proangiogenic myeloid cell inflammatory infiltrate promote CNV in neovascular AMD, although direct evidence for this hypothesis is missing. Eyes from VEGF-A^{hyper} mice showed focal early vacuolar degeneration of RPE cells already at ~4–6 weeks of age, whereas overlying photoreceptors were intact (Figures 5A and S3C). The first-observed changes in the retina overlying RPE defects showed migration of retinal Muller glia cells toward sites of RPE degeneration (Figure 5A), which dramatically accumulated with progressive age at sites of RPE defects and replaced photoreceptors (Figure 5B). Subsequently, progressive formation of CNV lesions was observed at sites of increased RPE degeneration, starting in young mice and progressing to large confluent multifocal CNV lesions in aged mice (Figures 3A–3D and S3I –S3K). The proliferating new vessels in CNV lesions were perfused through the choroidal vasculature (Figures 3A and 3B). RPE cells overlying CNV lesions showed increased RPE barrier breakdown with cytoplasmic β-catenin accumulation (Figures 3F, S3K, and S3L) and degenerative atrophic changes (Figures S3A and S3B), linking RPE barrier breakdown with CNV formation.

CNV lesions in VEGF-A^{hyper} mice showed striking resemblance to neovascular AMD lesions in humans with the formation of neovascular membranes and loss of the overlying photoreceptors (Figures 3C–3E). Although the photoreceptor layer was attenuated throughout the retina with increasing age associated with RPE degenerative changes, a cardinal feature of nonexudative AMD, a complete loss of the photoreceptor layer was limited to the retina overlying CNV lesions (Figures 3D and 5B), as is typically seen in neovascular AMD. At sites of CNV lesion formation, retinal Muller glia cells completely replaced photoreceptors with progressive age (Figure 5B). Thus, VEGF-A^{hyper} mice develop cardinal features of both nonexudative and neovascular AMD with progressive age.

NLRP3 Inflammasome Activation in Mice with Increased VEGF-A Levels

To identify molecular mechanisms that promote the AMD-like pathologies in aged VEGF-A^{hyper} mice, RPE cells were isolated from eyes of aged VEGF-A^{hyper} mice and control littermate mice for gene expression-profiling experiments. Among the highly upregulated genes in the RPE of VEGF-A^{hyper} mice were the inflammasome component NLRP3, IL-1β, and the complement cascade component C1q (Table S1). It has recently been reported that the NLRP3 inflammasome is activated in AMD, but the significance of NLRP3 inflammasome activation for the pathogenesis of AMD is not known and has not been validated in an animal model that reflects the human disease process (Kaneko et al., 2011; Tarallo et al., 2012; Doyle et al., 2012). The complement pathway component C1q, found in drusen in AMD, has been shown to activate the NLRP3 inflammasome in peripheral blood mononuclear cells in vitro, but whether NLRP3 inflammasome activation in macrophages plays a pathogenic role for AMD has not been shown (Doyle et al., 2012). Fatty acids have also been shown to be able to activate the NLRP3 inflammasome, and these lipids are also found in drusen and basal laminar deposits in AMD (Curcio et al., 2005a; Duewell et al., 2010; Wen et al., 2011). Similarly, the basal laminar sub-RPE deposits in aged VEGF-A^{hyper} mice showed evidence for lipid deposition by electron microscopy and oil red O staining (which binds triglycerides, esterified cholesterols, and fatty acids) (Figure 2I), which may promote inflammasome activation in the RPE of these mice.

Cell PRESS
Open ACCESS

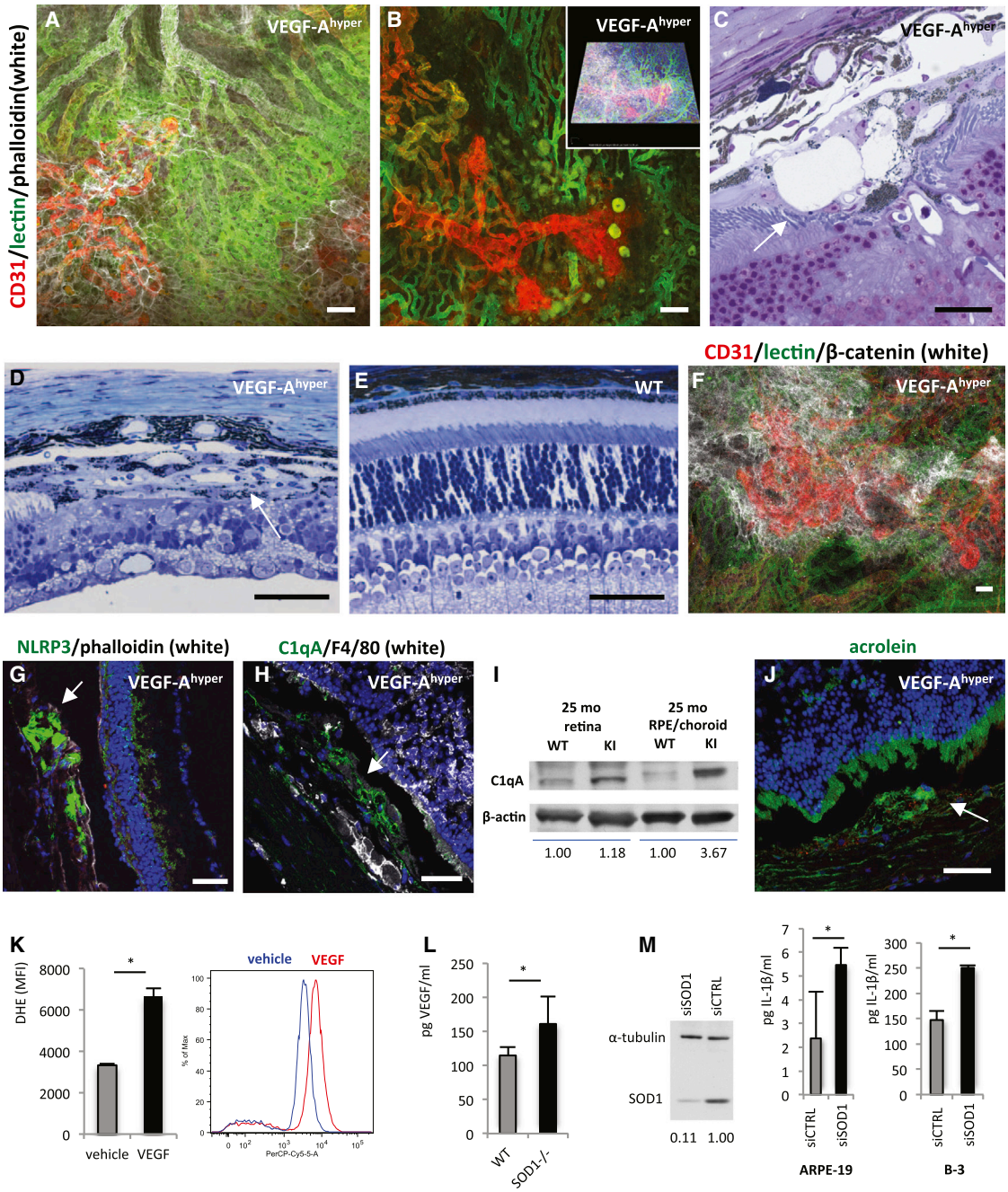

Figure 3. CNV and NLRP3 Expression in Aged VEGF-A^{hyper} Mice

(A and B) Perfusion experiments in aged white VEGF-A^{hyper} mice with fluorescein-conjugated tomato lectin and subsequent whole-mount staining for CD31 and phalloidin show that proliferating neovessels (CD31, red) originate from the underlying perfused choroidal vasculature (green) and extend into the sub-RPE space. Autofluorescent round deposits can be seen at sites of CNV lesions. Scale bars, 50 μm. Inset in (B) represents modeled z-stack of lesion.

(C) Representative section of CNV lesion in aged VEGF-A^{hyper} mice shows massive subretinal neovascularization (arrow). Scale bar, 20 μm.

(D) Representative image of a fully formed CNV lesion in a 7-month-old VEGF-A^{hyper} mouse that resembles a neovascular membrane in neovascular AMD (arrow). Neovascularization and fibrosis have completely replaced the photoreceptor layer at the site of CNV formation. Scale bar, 50 μm.

(E) In age-matched control littermate mice, such lesions were not seen. Scale bar, 50 μm.

(F) Colocalization of RPE barrier breakdown with CNV lesions. Choroidal flat mount of a 24-month-old white VEGF-A^{hyper} mouse in which choroidal perfusion is assessed by intracardiac administration of a fluorescein-conjugated tomato lectin (green). Subsequent whole-mount staining for CD31 (red) highlights proliferating neovessels from underlying perfused choroidal vessels (green), and labeling for β-catenin (white) shows RPE barrier breakdown at sites of neovascularization with cytoplasmic accumulation of β-catenin. Scale bar, 50 μm.

(legend continued on next page)

Immunostaining showed strong NLRP3 expression in RPE cells predominantly within CNV lesions in VEGF-A^{hyper} mice (Figures 3G and S4A), linking increased RPE barrier breakdown and RPE degeneration with NLRP3 inflammasome activation and subsequent neovascularization. In addition, strong accumulation of C1q was observed in a perivascular pattern in CNV lesions (Figures 3H and 3I), consistent with the gene expression-profiling results and its reported role as an NLRP3 inflammasome activator.

In ARPE-19 cells, oxidative stress can activate the NLRP3 inflammasome (Kauppinen et al., 2012). Notably, VEGF-A has been shown to induce oxidative stress in endothelial cells, whereas challenging RPE cells in vitro with oxidants increased VEGF-A levels (Klettner and Roider, 2009; Monaghan-Benson and Burridge, 2009). Consistent with these observations, VEGF-A treatment resulted in a rapid and significant increase of oxidative stress (determined by measuring superoxide reaction with dihydroethidium) in ARPE-19 cells (Figure 3K), and staining for acrolein (a marker for oxidative damage-induced lipid peroxidation) (Dorrell et al., 2009) was increased focally in RPE cells of aged VEGF-A^{hyper} mice (Figure 3J), suggesting that a chronic increase of VEGF-A results in increased oxidative damage in RPE cells.

Mice with deficiency of the antioxidant enzyme SOD1, resulting in increased superoxide levels, develop with progressive age RPE barrier breakdown and some AMD-like pathologies, albeit much more delayed and less striking than VEGF-A^{hyper} mice (Imamura et al., 2006). Because oxidative stress results in an increase in VEGF-A levels in RPE cells in vitro, and SOD1 null mice phenocopy to some degree VEGF-A^{hyper} mice, it is possible that the observed AMD-like pathologies in SOD1 null mice may be mediated in part by increased VEGF-A levels. Indeed, VEGF-A serum levels in young SOD1 null mice, prior to the manifestation of AMD-like pathologies, were increased compared to control littermate mice (Figure 3L), further suggesting that increased VEGF-A levels are central to the development of AMD-like pathologies. Oxidative stress induced by SOD1 knockdown in ARPE-19 cells (as well as in a lens epithelial cell line) resulted in increased IL-1β levels in the cell culture supernatant (Figure 3M), demonstrating a contributory role of oxidative stress to inflammasome activation in RPE cells as well.

Thus, degenerative RPE changes following VEGF-A-induced RPE barrier breakdown in VEGF-A^{hyper} mice are associated with increased sub-RPE lipid and complement C1q deposits and increased oxidative damage, all factors promoting inflammasome activation. To test whether in VEGF-A^{hyper} mice NLRP3 inflammasome activation occurs, the protein levels of the active caspase-1 subunits p10 and p20 were examined, which are derived from caspase-1 precursor through autocatalytic cleavage when the inflammasome is activated. Western blotting confirmed activation of the inflammasome with increased p10 and p20 active subunits in RPE/choroid tissues of aged VEGF-A^{hyper} mice, whereas control littermate mice showed no inflammasome activation (Figure 4A). Furthermore, immunostaining showed coexpression of NLRP3 and p10 focally in the RPE/choroid of aged VEGF-A^{hyper} mice, consistent with NLRP3 inflammasome activation (Figures 4B, S4B, and S4C).

Choroidal flat mounts from aged VEGF-A^{hyper} mice showed that increased NLRP3 expression was limited to degenerative RPE cells that had lost their typical honeycomb appearance, whereas no NLRP3 expression was seen in normal-appearing adjacent RPE cells or macrophages (Figures 4C and S4D). Notably, NLRP3 expression and degenerative changes of RPE cells were often seen in association with a large number of round extracellular autofluorescent deposits that were phalloidin negative (average diameter, 25.6 ± 6.8 μm; average area, 574.8 ± 190.8 μm) (Figures 4D–4G).

Targeting the NLRP3 Inflammasome Inhibits AMD-like Pathologies in VEGF-A^{hyper} Mice

To test whether NLRP3 inflammasome activation in VEGF-A^{hyper} mice contributes to VEGF-A-induced AMD pathologies, NLRP3 or the inflammasome effector cytokines IL-1β and IL-18 were targeted genetically in VEGF-A^{hyper} mice. NLRP3, IL-1 receptor type 1, and IL-18 null mice showed no AMD-like pathologies. Notably, targeting NLRP3, IL-1 receptor type 1 (abolishing IL-1β signaling), or IL-18 in VEGF-A^{hyper} mice did not prevent the observed chorioretinal pathologies, and double-mutant mice showed RPE barrier breakdown, RPE degeneration, and multifocal CNV lesions with macrophage infiltration as seen in VEGF-A^{hyper} mice (Figures 4H and S4E–S4G). However, deficiency of NLRP3 or IL-1 receptor type 1 in VEGF-A^{hyper} mice

(G) Strongly increased NLRP3 expression in the RPE/choroid (arrow) with attenuation or loss of the overlying photoreceptor layer in a 15-month-old VEGF-A^{hyper} mouse. Scale bar, 50 μm.

(H) Perivascular accumulation of C1qA within CNV lesions (arrow). A 15-month-old VEGF-A^{hyper} mouse is shown. Scale bar, 50 μm.

(I) Western blotting demonstrates accumulation of C1qA in choroid/RPE tissues of aged VEGF-A^{hyper} mice, whereas control littermate mice showed no accumulation of C1qA. Choroid/RPE or retinal tissues represent pools from three 25-month-old VEGF-A^{hyper} mice or control mice. Normalized relative densitometric values are indicated.

(J) Acrolein, a marker for ROS-induced lipid peroxidation, is increased focally in abnormal RPE cells in aged VEGF-A^{hyper} mice (green, arrow) (15 months old). DAPI nuclear staining was performed; photoreceptor outer segments show autofluorescence (green). Scale bar, 50 μm.

(K) VEGF-A^{165} treatment of ARPE-19 cells loaded with 10 μM dihydroethidium (DHE) induces increased oxidative stress (superoxide indicator), measured by FACS (PerCP-Cy5.5 channel). y Axis shows mean fluorescence intensity (MFI) of triplicate experiments (n = 3/group). A representative histogram demonstrates the shift of fluorescence induced by VEGF-A^{165}, representing increased superoxide species. Error bars, mean ± SD. *p < 0.05.

(L) VEGF-A serum levels are increased in young (7 weeks old) SOD1$^{-/-}$ mice compared to age- and gender-matched control littermate mice (n = 5). Error bars, mean ± SD. *p < 0.05.

(M) SOD1 is efficiently depleted using SOD1-targeted siRNA, demonstrated by western blotting of ARPE-19 cell lysate. Cell culture supernatant of cells, primed with 4 ng/ml IL-1α, shows that SOD1 knockdown increases levels of the inflammasome effector cytokine IL-1β in both ARPE-19 cells and the B-3 lens epithelial cells (n = 4/group). Error bars, mean ± SD. *p < 0.05.

See also Figure S3.

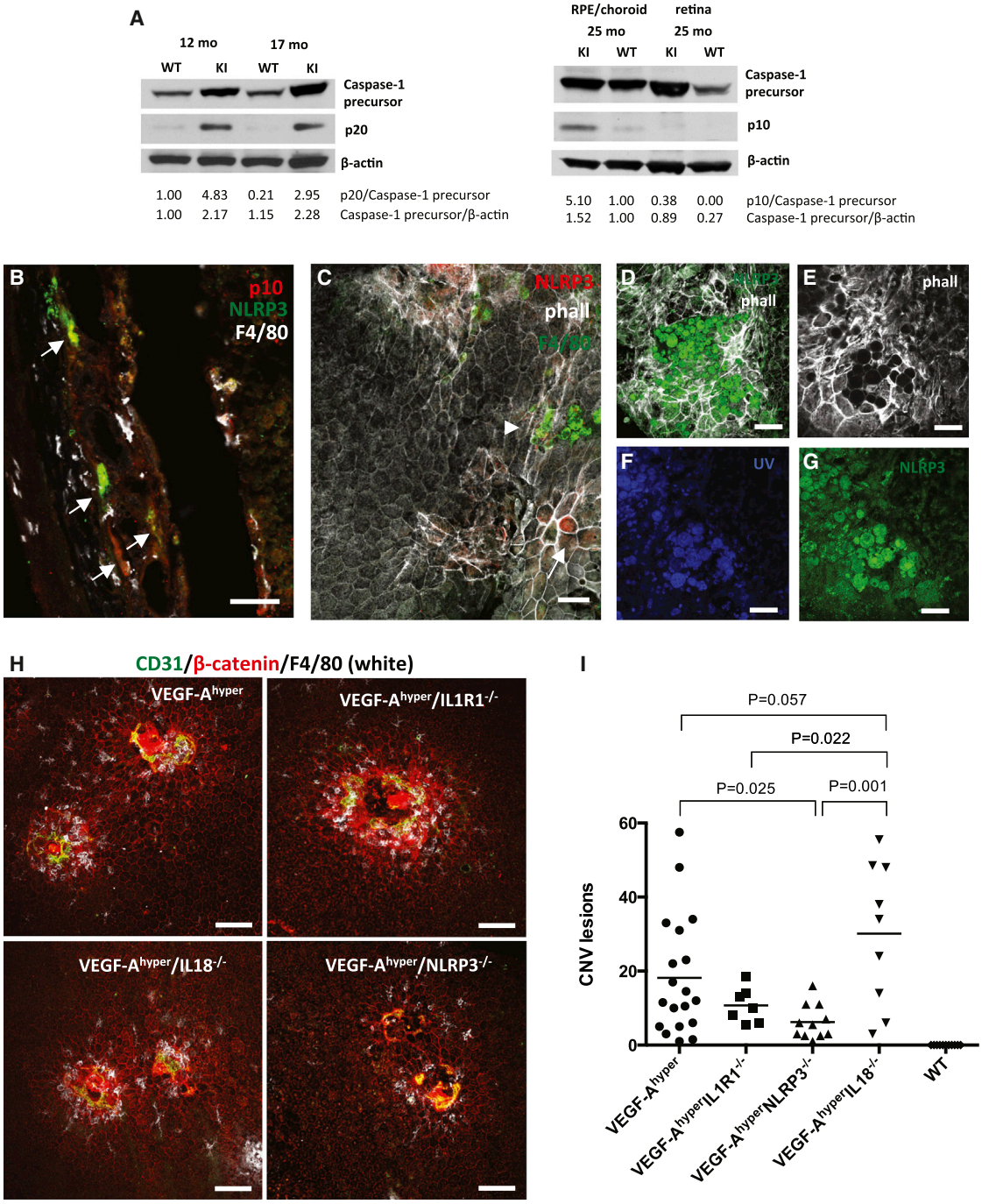

Figure 4. Blockade of the NLRP3 Inflammasome Reduces CNV Lesions in VEGF-A^{hyper} Mice

(A) Left: western blotting of posterior eye lysates from 12- and 17-month-old VEGF-A^{hyper} mice (KI) and control littermate mice (WT) shows activation of the inflammasome with strong upregulation of the caspase-1 active subunit p20 in mutant mice. Right: pools of RPE/choroid or retinal tissue from three 25-month-old VEGF-A^{hyper} mice (KI) and control littermate mice (WT) show strong upregulation of the p10 caspase-1 active subunit in the RPE/choroid, but not in the retina, demonstrating inflammasome activation in RPE/choroid tissues of VEGF-A^{hyper} mice. Normalized densitometric values are indicated.

(B) NLRP3 (green, arrows) is strongly expressed in the RPE/choroid in VEGF-A^{hyper} mice (15 months old). Macrophages are stained with F4/80 (white). Colabeling for the activated p10 subunit of caspase-1 (red) with NLRP3 (green) shows inflammasome activation. Scale bar, 50 μm.

(C) NLRP3 immunostaining of choroidal flat mounts with expression of NLRP3 in RPE cells that show abnormal cellular morphology (phalloidin [phall], white; arrow), whereas normal-appearing RPE cells with typical honeycomb cytoarchitecture do not express NLRP3 (red) (13 months old). No NLRP3 expression is seen in F4/80^{+} macrophages (green, arrowhead). Scale bar, 50 μm.

(legend continued on next page)

reduced the number of CNV lesions that formed in 6-week-old mice, whereas deficiency in IL-18 resulted in a significantly increased number of CNV lesions compared to double-mutant VEGF-A^{hyper} mice lacking IL-1R1 or NLRP3 (Figure 4I). VEGF-A protein levels in the RPE/choroid, retina, or serum were not increased in IL-18 null mice compared to NLRP3 or IL-1R1 null mice, suggesting that IL-18 deficiency promotes CNV lesion formation through VEGF-A-independent mechanisms (data not shown). Thus, NLRP3 inflammasome activation and the resulting increase in active IL-1β, which acts as a potent proangiogenic factor, promote VEGF-A-induced AMD pathologies, such as RPE barrier breakdown and CNV lesion formation.

Macrophages Activate Proangiogenic Retinal Glia Cells to Promote CNV

To determine which cell types are critical for promoting CNV, the spatiotemporal cellular events that lead to CNV lesion formation in VEGF-A^{hyper} mice were analyzed. Retinal Muller cell accumulation and increased glial fibrillary acid protein (GFAP) expression occur in human AMD retinas, but the significance of these Muller cells for AMD pathogenesis is not known (Wu et al., 2003). Eyes of VEGF-A^{hyper} mice showed a progressive increase of GFAP expression in retinal cells overlying evolving CNV lesions (Figures 5C–5F). In young mutant mice at sites of accumulation of a myeloid cell infiltrate between the RPE and the retina, GFAP expression in cells of the overlying retina was increased, and Muller cells migrated toward the RPE prior to neovessel formation (Figure 5C). Strong GFAP staining and retinal Muller cell accumulation were observed subsequently in evolved CNV lesions (Figures 5D and 5E). Increased N-cadherin expression was also observed in Muller cells at sites of evolving CNV lesions, a marker for proliferating glia cells (Figure S5H). These findings suggest that RPE barrier breakdown and macrophage infiltration into the space between the retina and the RPE occur first and that these macrophages subsequently activate retinal Muller glia cells to promote CNV.

Although infiltrating macrophages in VEGF-A^{hyper} mice do not stain for VEGF-A (β-gal^{-}), RPE cells in CNV lesions strongly expressed VEGF-A (Figures 5I and S3E). Overlying retinal glia cells that infiltrated CNV lesions strongly expressed VEGF-A as well (Figures 5H and 5I). Furthermore, these cells showed high expression of the proangiogenic cytokine IL-1β and of IL-18, and colabeling for GFAP confirmed that these cells were retinal Muller glia cells (Figures 5G–5K and S5A–S5D). Choroidal flat mounts, in which the retina was removed, showed glia Muller cells adhering to the RPE and infiltrating CNV lesions and that these cells were the main source of IL-1β in CNV lesions (Figure S5E). Glia cells infiltrated degenerative RPE cells particularly at sites with high density of autofluorescent sub-RPE deposits (Figures S5G and S5I).

The observations in CNV formation in VEGF-A^{hyper} mice suggest that RPE defects and barrier breakdown are followed by a macrophage infiltrate into the space between the retina and the RPE that activates retinal Muller glia cells, which promote CNV through secretion of proangiogenic factors including VEGF-A and IL-1β. If this sequence of events is required for neovascularization, ablation of the myeloid cell infiltrate should result in reduced glia cell activation and inhibition of subsequent neovascularization. This hypothesis was tested in a laser injury model of CNV, in which disruption of the RPE barrier is achieved through a laser that targets the pigmented RPE cells and leads to subsequent CNV lesions through proliferation of blood vessels at the site of laser injury. Although this acute injury model is limited in the assessment of the role of chronic changes for AMD pathogenesis, it allows the characterization of acute spatiotemporal events during neovascularization in the choroid (He and Marneros, 2013). Similar to CNV lesion formation in VEGF-A^{hyper} mice, time course experiments showed that in the laser injury model of CNV, macrophages infiltrate the site of laser injury early, followed by the formation of a NG2^{+}SMA^{+} myofibroblastic scaffold into which Muller glial cells infiltrate, before neovascularization occurs (Figures 6A–6G). Like in CNV lesions in VEGF-A^{hyper} mice, VEGF-A expression could not be detected in macrophages in laser-induced CNV lesions, but VEGF-A expression was seen in RPE cells as well as glia cells overlying CNV lesions, which also expressed IL-1β (Figures S6A–S6D). Low-level NLRP3 expression was observed only in a few RPE cells in laser lesions, and not in lesional macrophages (Figures S6E and S6F). NLRP3 protein levels in lysates from pooled choroids of wild-type (WT) mice 3 days after laser injury were much lower and almost undetectable when compared to choroid lysates from age-matched unlasered VEGF-A^{hyper} mice (Figure S6G), suggesting that VEGF-A^{hyper} mice are better suited to investigate the role of the NLRP3 inflammasome for CNV than the laser injury-wounding model.

Macrophage populations after wound injury undergo an M2-like polarization with expression of the prototypic M2-macrophage marker Arg1. Consistent with the CNV laser injury model representing an acute wound-healing model of neovascularization, immunolabeling for Arg1 and F4/80 confirmed that most macrophages that accumulate at sites of laser injury are Arg1^{+}F4/80^{+} M2-like macrophages, whereas nonlesional choroidal F4/80^{+} cells were Arg1^{-} (Figure S6H). In human AMD eyes, a mixed macrophage infiltrate has been reported, with both M1 and M2 macrophage populations occurring (Cao et al., 2011). Similarly, only a subset of macrophages in

(D–G) Round autofluorescent extracellular deposits accumulate at sites of RPE degeneration in aged VEGF-A^{hyper} mice (21 months old). These round deposits are phalloidin negative (E) and show autofluorescence with UV light (F), or the green light channel (G), which also shows increased NLRP3 immunostaining at sites of these deposits. Scale bars, 50 μm.

(H) RPE barrier breakdown (β-catenin, red), macrophage infiltration (F4/80, white), and CNV lesion formation (CD31, green) occur in VEGF-A^{hyper} mice, despite genetic inactivation of IL-1R1, NLRP3, or IL-18 in these mice. Representative images of choroidal flat mounts from 6-week-old mice are presented. Scale bars, 100 μm.

(I) Quantitative analysis of CNV lesion numbers per age-matched mutant mice (6 weeks old) in choroidal flat mounts (average CNV lesion numbers/mouse of choroidal flat mounts stained for β-catenin and CD31). No CNV lesions were seen in WT control mice. p values were determined with a two-tailed Student's t test ($n > 7$ mice/group).

See also Figure S4.

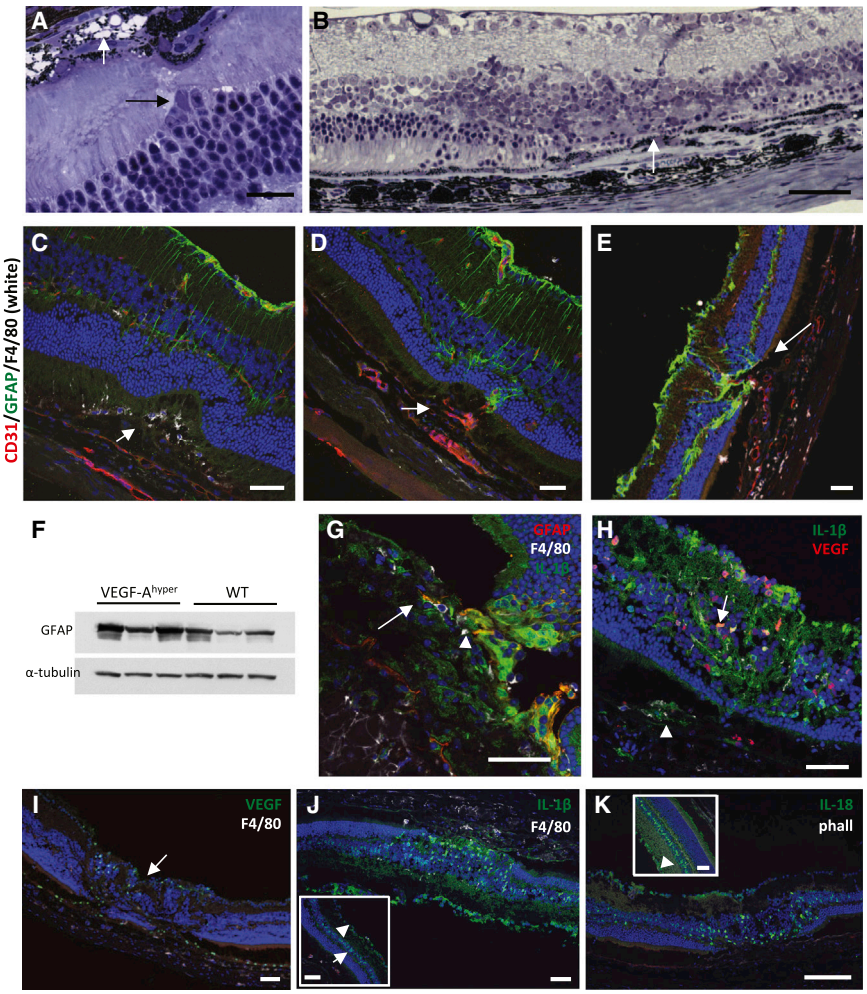

Figure 5. Glia Cell Activation in CNV Lesions in VEGF-A^{hyper} Mice

(A) In young VEGF-A^{hyper} mice (6 weeks old), early RPE degeneration is seen only focally with some RPE cells undergoing vacuolar degeneration (intracellular vacuoles with remaining pigment granules; white arrow). At this stage, retinal changes are limited, but migration of retinal Muller glia cells (black arrow) toward sites of RPE degeneration can already be observed. Scale bar, 20 μm.

(B) In aged VEGF-A^{hyper} mice, the photoreceptor layer adjacent to CNV lesions is present, but attenuated. Complete loss of photoreceptors is seen in retina overlying CNV lesions with an accumulation of retinal Muller glia cells (arrow). Scale bar, 50 μm. A 21-month-old VEGF-A^{hyper} mouse is shown.

(C) At sites of early evolving CNV lesions, subretinal macrophages (F4/80^{+}, white; arrow) are seen prior to neovessel formation. Limited to the overlying retina GFAP expression (green) increases, indicating glia cell activation and proliferation, whereas adjacent retina appears unchanged. Scale bar, 50 μm. A 4-month-old VEGF-A^{hyper} mouse is shown.

(D) In early CNV lesions with subretinal neovascularization (CD31, red; arrow), GFAP^{+} glia cells have increased and have infiltrated early CNV lesions (green). Scale bar, 50 μm. A 4-month-old VEGF-A^{hyper} mouse is shown.

(E) In aged VEGF-A^{hyper} mice with large CNV lesions, massive GFAP expression and glia cell infiltration into sites of CNV lesion formation are seen (arrow). Scale bar, 50 μm. A 15-month-old VEGF-A^{hyper} mouse is shown.

(F) Retinal GFAP is increased in aged VEGF-A^{hyper} mice compared to littermate control mice. 16-month-old mice are shown.

(G) Coimmunolabeling for GFAP (red), IL-1β (green), and F4/80 (white) shows that high IL-1β expression is seen in infiltrating retinal glia cells (arrowhead), whereas lower levels are observed in RPE cells and only in a few macrophages in CNV lesions (arrow). No IL-1β is detected in most choroidal macrophages. Scale bar, 50 μm. A 15-month-old VEGF-A^{hyper} mouse is shown.

(H) Retinal glia cells coexpress both VEGF-A and IL-1β in the retina overlying CNV lesions where the photoreceptor layer is severely attenuated (arrow). Labeling for IL-1β and VEGF-A is also seen in RPE cells (arrowhead) in CNV lesions. Scale bar, 50 μm. A 15-month-old VEGF-A^{hyper} mouse is shown.

(I) Increased VEGF-A expression (green) is seen in retinal glia cells overlying CNV lesions (arrow). Scale bar, 50 μm. A 15-month-old VEGF-A^{hyper} mouse is shown.

(J) Although IL-1β is expressed in glia cells overlying CNV lesions that have replaced the ONL, adjacent normal-appearing retina (inset) shows only weak IL-1β expression in the INL (arrow) and GCL (arrowhead). Scale bars, 50 μm. A 15-month-old VEGF-A^{hyper} mouse is shown.

(K) Infiltrating retinal glia cells show strong expression of IL-18 overlying CNV lesions. Inset shows IL-18 expression in normal retina to be prominent in the INL (arrowhead). Scale bar, 50 μm. A 15-month-old VEGF-A^{hyper} mouse is shown.

See also Figure S5.

spontaneous CNV lesions in aged VEGF-A^{hyper} mice was Arg1^{+} (Figure S6I), reflecting the mixed macrophage populations in human AMD eyes, which is consistent with a chronic progressive eye pathology.

Next, mutant mice were generated in which temporal ablation of macrophages can be induced through injection of diphtheria toxin (Lysozyme M Cre-iDTR homozygous mice). Selective temporal ablation of macrophages in these mice inhibited the formation of the SMA^{+}NG2^{+} myofibroblastic scaffold and glia cell accumulation in laser lesions and reduced subsequent neovascularization significantly (Figures 6H–6O). Thus, macrophages promote glia cell activation (with activated glia cells expressing proangiogenic VEGF-A and IL-1β) and subsequent CNV.

DISCUSSION

The findings in aged VEGF-A^{hyper} mice reveal that a chronic increase in VEGF-A levels is sufficient to cause age-dependent cardinal features of both nonexudative AMD and neovascular AMD, providing a unifying pathomechanism for advanced AMD. These features are likely to be a consequence of both direct as well as indirect effects of increased VEGF-A signaling, such as through the induction of downstream pathways and cellular changes. The findings are consistent with the clinical observation that neovascular AMD can often co-occur with nonexudative AMD and highlight the notion that AMD can occur along a spectrum with the manifestations of features of

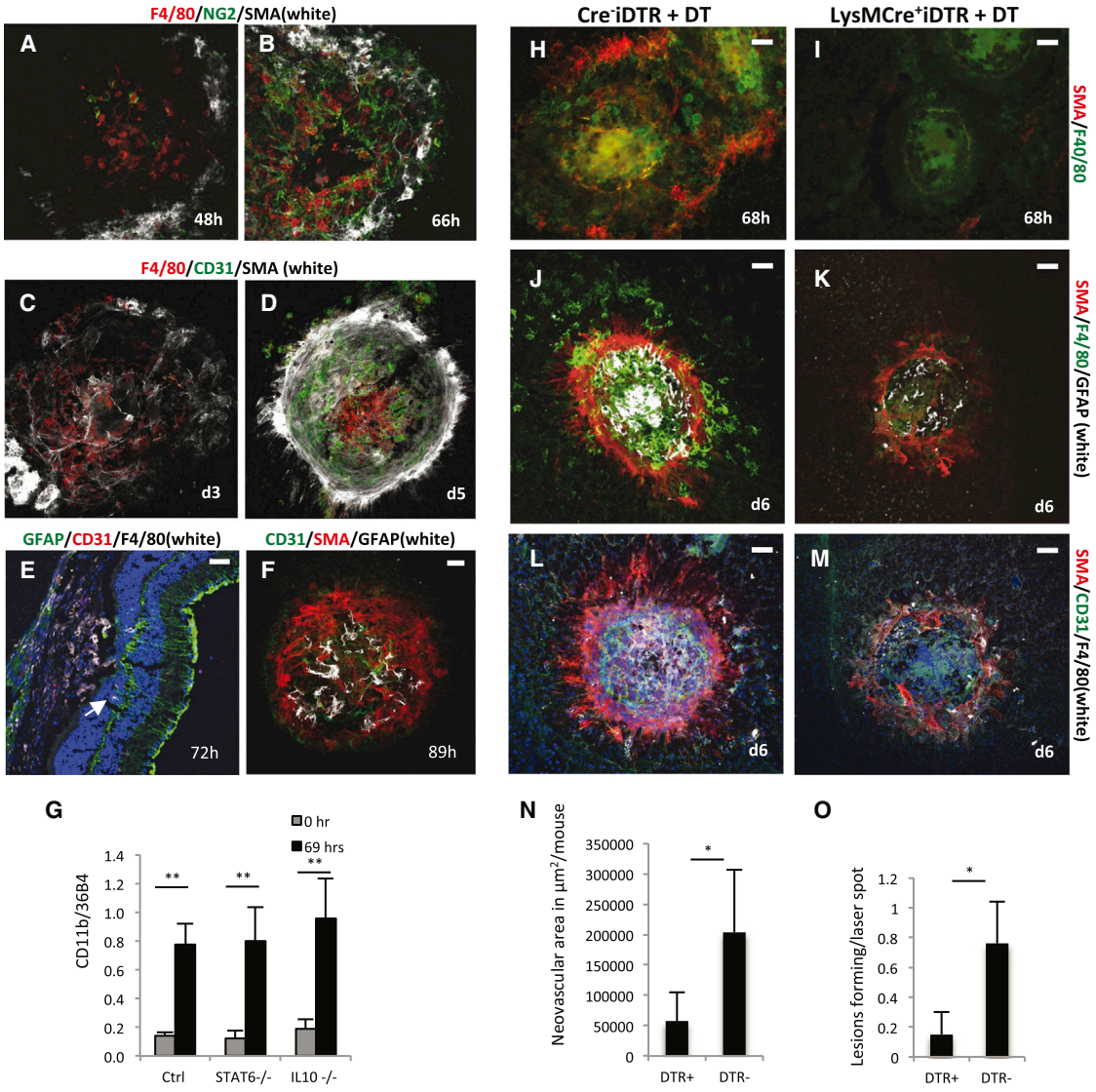

Figure 6. Macrophages Are Required for Retinal Glia Cell Activation and Subsequent Neovascularization

(A and B) A fibroblast-like scaffold forms after macrophage (red) infiltration that is positive for NG2 (green) and SMA (white). 10× magnification.

(C) The fibroblast-like scaffold forms prior to infiltration of the laser injury site with endothelial cells because the first $CD31^+$ endothelial cells are seen at about 68 hr after injury, when the $NG2^+SMA^+$ scaffold has already formed. 10× magnification.

(D) Neovascularization occurs after macrophage infiltration and after the formation of the SMA^+ scaffold, and fully formed CNV lesions are seen at day 5 (CD31, green). The SMA^+ scaffold covers the neovascular lesions, resembling a scar after wound injury. 10× magnification. Control mice are shown.

(E) $GFAP^+$ retinal glia cells (arrow) infiltrate the laser injury site already by 72 hr after laser injury, before endothelial cells have populated the site. Scale bar, 50 µm.

(F) At day 4 after laser injury, new blood vessels form at the site of laser injury after $GFAP^+$ cells have already infiltrated the SMA^+ scaffold. Scale bar, 50 µm. Control mice are shown in (A)–(F).

(G) Semiquantitative RT-PCR of choroidal tissue lysates shows an increase of macrophages at 69 hr after laser injury (CD11b levels normalized to 36B4 housekeeping gene), consistent with the immunolabeling results. Macrophage accumulation occurs independently of IL10 or STAT6 signaling (n = 5/group). Error bars, mean ± SD. **$p < 0.01$. Ctrl, control.

(H and I) Homozygous $LysMCre^+$iDTR mice were used for DT injections to temporally and selectively ablate myeloid cells in laser injury experiments and compared to Cre^-iDTR mice. DT treatment potently diminished $F4/80^+$ macrophage infiltration into the laser injury site, assessed here at 68 hr after injury. Ablation of macrophages also inhibited the SMA^+ scaffold formation (I).

(J and K). Ablation of macrophages inhibited $GFAP^+$ glia cell activation (white) and infiltration into the site of laser injury.

(L and M) Inhibition of macrophage infiltration and glia cell activation resulted in a significant inhibition of neovascularization. Only few $CD31^+$ vessels (green) were seen at laser injury sites in which macrophage accumulation was reduced, whereas full neovascular lesions formed in mice with no ablation of macrophages. Scale bars, 50 µm.

(N and O) Reduced CNV lesion formation was seen in mice with selective ablation of macrophages, with a reduction in the total neovascular area and the rate of CNV lesion formation for each laser injury administered (n = 20 mice/group). Error bars, mean ± SD. *$p < 0.05$.

See also Figure S6.

both neovascular and nonexudative forms (Sunness et al., 1999).

AMD has been proposed to be a multifactorial disease, and various risk factors for AMD have been identified, including smoking, advanced age, chronic light exposure, and genetic risk factors (Friedman et al., 2004; Klein et al., 2004; van Leeuwen et al., 2003). The observations of cardinal features of AMD in aged VEGF-A^{hyper} mice that only differ from their control littermates by increased VEGF-A levels suggest that in AMD multiple risk factors may converge to cause mainly RPE hypoxia and oxidative damage, which stimulate increased VEGF-A expression in RPE cells (Klettner and Roider, 2009). Thus, although advanced AMD may result from multifactorial insults to the RPE in humans, aged VEGF-A^{hyper} mice serve as a mouse model for AMD due to a single genetic alteration that leads to increased VEGF-A levels, demonstrating a central role of increased VEGF-A signaling in AMD pathogenesis. The observation in VEGF-A^{hyper} mice that early RPE degenerative changes are seen prior to photoreceptor loss provides in vivo evidence that the RPE is at the center of the disease process in AMD and that retinal degeneration occurs as a consequence of an impaired RPE function.

Increased VEGF-A levels are shown here to lead to RPE barrier breakdown and progressive degenerative changes in the RPE, which are associated with accumulation of lipid-rich basal laminar sub-RPE deposits and complement C1q, and an increase in oxidative damage, similarly as in human eyes with AMD. These RPE abnormalities are linked to NLRP3 inflammasome activation, focal RPE cell death, and CNV lesion formation. Targeting NLRP3 or IL-1β signaling in these mice reduced RPE barrier breakdown and CNV lesion formation, demonstrating that the NLRP3 inflammasome contributes to VEGF-A-induced AMD-like pathologies. IL-18 deficiency had an opposite effect on CNV lesion formation, suggesting an antiangiogenic effect of IL-18 (Doyle et al., 2012). Although NLRP3 deficiency increased the size of laser injury-induced neovascular lesions in an acute wound-healing model in the eye (Doyle et al., 2012), an inhibition of CNV lesion number was observed here in VEGF-A^{hyper} mice that lack NLRP3. These differences are not surprising, because in the acute laser injury model, neovascularization occurs in the setting of healthy RPE cells that show little or no NLRP3 expression, and it occurs within 4 days after injury. In contrast, CNV lesions in VEGF-A^{hyper} mice develop over a prolonged period of time and occur in the setting of RPE barrier breakdown and VEGF-A associated accumulation of C1q and oxidative damage, with strong expression of NLRP3 and inflammasome activation, similar to human AMD.

It is further shown here that RPE barrier breakdown leads to accumulation of macrophages into the space between the RPE and the retina, with subsequent activation of retinal Muller glia cells that strongly express the proangiogenic factors IL-1β and VEGF-A to promote CNV. These findings are consistent with observations that showed human neovascular AMD lesions to contain a large number of IL-1β-expressing cells and RPE cells to express VEGF-A (Oh et al., 1999).

In summary, aged VEGF-A^{hyper} mice serve as an important new mouse model for both forms of AMD and reveal a central role of increased VEGF-A and NLRP3 inflammasome activation for RPE degeneration and AMD pathogenesis. Preventative strategies to reduce RPE hypoxia or therapeutically target increased VEGF-A signaling in combination with blocking IL-1β or the NLRP3 inflammasome could therefore inhibit both forms of AMD.

EXPERIMENTAL PROCEDURES

Animals

The generation of VEGF-A^{hyper} mice and VEGF-A^{hypo} mice was previously reported by Miquerol et al. (1999) and Damert et al. (2002). VEGF-A^{hyper} mice were crossed with IL-18$^{-/-}$, IL-1R1$^{-/-}$, or NLRP3$^{-/-}$ mice to obtain mice that are heterozygous for the VEGF-A^{hyper} allele and homozygous null for IL-18, IL-1R1, or NLRP3 (Jackson Laboratory) (Takeda et al., 1998; Glaccum et al., 1997; Brydges et al., 2009).

Immunolabeling

Eyes were fixed in 4% paraformaldehyde. For choroidal flat mounts, eyes were permeabilized in 0.5% Triton X-100 and subsequently blocked with 5% serum in which the secondary antibodies were raised. A full description of antibodies used is provided in the Extended Experimental Procedures. Staining for β-gal activity was performed as described previously (Marneros et al., 2005).

Western Blotting

Eye tissues from VEGF-A^{hyper} mice and control littermate mice of different ages were used for western blotting experiments. Freshly dissected posterior eye poles were lysed in NP40 lysis buffer with 1 mM PMSF and protease inhibitor cocktail using the QIAGEN TissueLyser II. After centrifugation, the supernatant was used for western blotting. A full description of antibodies used is provided in Extended Experimental Procedures.

Experimental CNV Model

Eyes of age- and gender-matched mice were exposed to laser photocoagulation for induction of experimental CNV after eyes were dilated with 1% tropicamide and mice were anesthetized with 75 mg/kg ketamine and 7.5 mg/kg xylazine. Laser photocoagulation was performed using a 532 nm laser (Zeiss; VISULAS 532s). Lesions were induced using a power of 200 mW, a spot size of 50 μm, and a duration of 100 ms as previously described (He and Marneros, 2013).

SUPPLEMENTAL INFORMATION

Supplemental Information includes Extended Experimental Procedures, six figures, and one table and can be found with this article online at http://dx.doi.org/10.1016/j.celrep.2013.08.002.

ACKNOWLEDGMENTS

I would like to thank Drs. Andras Nagy, Lucile Miquerol, and Annette Damert for providing VEGF-A^{hyper} and VEGF-A^{hypo} mice and Dr. Napoleone Ferrara for providing VEGF-A$^{fl/fl}$ mice. This work was supported by a grant to A.G.M. from the NEI R01-EY019297.

Received: June 13, 2013
Revised: July 16, 2013
Accepted: August 8, 2013
Published: August 29, 2013

REFERENCES

Ablonczy, Z., Dahrouj, M., Tang, P.H., Liu, Y., Sambamurti, K., Marmorstein, A.D., and Crosson, C.E. (2011). Human retinal pigment epithelium cells as functional models for the RPE in vivo. Invest. Ophthalmol. Vis. Sci. *52*, 8614–8620.

Anderson, D.H., Mullins, R.F., Hageman, G.S., and Johnson, L.V. (2002). A role for local inflammation in the formation of drusen in the aging eye. Am. J. Ophthalmol. *134*, 411–431.

Bird, A.C., Bressler, N.M., Bressler, S.B., Chisholm, I.H., Coscas, G., Davis, M.D., de Jong, P.T., Klaver, C.C., Klein, B.E., Klein, R., et al.; The International ARM Epidemiological Study Group. (1995). An international classification and grading system for age-related maculopathy and age-related macular degeneration. Surv. Ophthalmol. *39*, 367–374.

Brydges, S.D., Mueller, J.L., McGeough, M.D., Pena, C.A., Misaghi, A., Gandhi, C., Putnam, C.D., Boyle, D.L., Firestein, G.S., Horner, A.A., et al. (2009). Inflammasome-mediated disease animal models reveal roles for innate but not adaptive immunity. Immunity *30*, 875–887.

Cao, X., Shen, D., Patel, M.M., Tuo, J., Johnson, T.M., Olsen, T.W., and Chan, C.C. (2011). Macrophage polarization in the maculae of age-related macular degeneration: a pilot study. Pathol. Int. *61*, 528–535.

Cervi, D., Shaked, Y., Haeri, M., Usenko, T., Lee, C.R., Haigh, J.J., Nagy, A., Kerbel, R.S., Yefenof, E., and Ben-David, Y. (2007). Enhanced natural-killer cell and erythropoietic activities in VEGF-A-overexpressing mice delay F-MuLV-induced erythroleukemia. Blood *109*, 2139–2146.

Curcio, C.A., Presley, J.B., Malek, G., Medeiros, N.E., Avery, D.V., and Kruth, H.S. (2005a). Esterified and unesterified cholesterol in drusen and basal deposits of eyes with age-related maculopathy. Exp. Eye Res. *81*, 731–741.

Curcio, C.A., Presley, J.B., Millican, C.L., and Medeiros, N.E. (2005b). Basal deposits and drusen in eyes with age-related maculopathy: evidence for solid lipid particles. Exp. Eye Res. *80*, 761–775.

Damert, A., Miquerol, L., Gertsenstein, M., Risau, W., and Nagy, A. (2002). Insufficient VEGFA activity in yolk sac endoderm compromises haematopoietic and endothelial differentiation. Development *129*, 1881–1892.

Dorrell, M.I., Aguilar, E., Jacobson, R., Yanes, O., Gariano, R., Heckenlively, J., Banin, E., Ramirez, G.A., Gasmi, M., Bird, A., et al. (2009). Antioxidant or neurotrophic factor treatment preserves function in a mouse model of neovascularization-associated oxidative stress. J. Clin. Invest. *119*, 611–623.

Doyle, S.L., Campbell, M., Ozaki, E., Salomon, R.G., Mori, A., Kenna, P.F., Farrar, G.J., Kiang, A.S., Humphries, M.M., Lavelle, E.C., et al. (2012). NLRP3 has a protective role in age-related macular degeneration through the induction of IL-18 by drusen components. Nat. Med. *18*, 791–798.

Duewell, P., Kono, H., Rayner, K.J., Sirois, C.M., Vladimer, G., Bauernfeind, F.G., Abela, G.S., Franchi, L., Nuñez, G., Schnurr, M., et al. (2010). NLRP3 inflammasomes are required for atherogenesis and activated by cholesterol crystals. Nature *464*, 1357–1361.

Friedman, D.S., O'Colmain, B.J., Muñoz, B., Tomany, S.C., McCarty, C., de Jong, P.T., Nemesure, B., Mitchell, P., and Kempen, J.; Eye Diseases Prevalence Research Group. (2004). Prevalence of age-related macular degeneration in the United States. Arch. Ophthalmol. *122*, 564–572.

Fritsche, L.G., Chen, W., Schu, M., Yaspan, B.L., Yu, Y., Thorleifsson, G., Zack, D.J., Arakawa, S., Cipriani, V., Ripke, S., et al.; AMD Gene Consortium. (2013). Seven new loci associated with age-related macular degeneration. Nat. Genet. *45*, 433–439, e1–e2.

Funk, M., Karl, D., Georgopoulos, M., Benesch, T., Sacu, S., Polak, K., Zlabinger, G.J., and Schmidt-Erfurth, U. (2009). Neovascular age-related macular degeneration: intraocular cytokines and growth factors and the influence of therapy with ranibizumab. Ophthalmology *116*, 2393–2399.

Glaccum, M.B., Stocking, K.L., Charrier, K., Smith, J.L., Willis, C.R., Maliszewski, C., Livingston, D.J., Peschon, J.J., and Morrissey, P.J. (1997). Phenotypic and functional characterization of mice that lack the type I receptor for IL-1. J. Immunol. *159*, 3364–3371.

He, L., and Marneros, A.G. (2013). Macrophages are essential for the early wound healing response and the formation of a fibrovascular scar. Am. J. Pathol. *182*, 2407–2417.

Imamura, Y., Noda, S., Hashizume, K., Shinoda, K., Yamaguchi, M., Uchiyama, S., Shimizu, T., Mizushima, Y., Shirasawa, T., and Tsubota, K. (2006). Drusen, choroidal neovascularization, and retinal pigment epithelium dysfunction in SOD1-deficient mice: a model of age-related macular degeneration. Proc. Natl. Acad. Sci. USA *103*, 11282–11287.

Jafarifar, F., Yao, P., Eswarappa, S.M., and Fox, P.L. (2011). Repression of VEGFA by CA-rich element-binding microRNAs is modulated by hnRNP L. EMBO J. *30*, 1324–1334.

Kaneko, H., Dridi, S., Tarallo, V., Gelfand, B.D., Fowler, B.J., Cho, W.G., Kleinman, M.E., Ponicsan, S.L., Hauswirth, W.W., Chiodo, V.A., et al. (2011). DICER1 deficit induces Alu RNA toxicity in age-related macular degeneration. Nature *471*, 325–330.

Kauppinen, A., Niskanen, H., Suuronen, T., Kinnunen, K., Salminen, A., and Kaarniranta, K. (2012). Oxidative stress activates NLRP3 inflammasomes in ARPE-19 cells—implications for age-related macular degeneration (AMD). Immunol. Lett. *147*, 29–33.

Klein, R., Peto, T., Bird, A., and Vannewkirk, M.R. (2004). The epidemiology of age-related macular degeneration. Am. J. Ophthalmol. *137*, 486–495.

Klettner, A., and Roider, J. (2009). Constitutive and oxidative-stress-induced expression of VEGF in the RPE are differently regulated by different Mitogen-activated protein kinases. Graefes Arch. Clin. Exp. Ophthalmol. *247*, 1487–1492.

Kliffen, M., van der Schaft, T.L., Mooy, C.M., and de Jong, P.T. (1997). Morphologic changes in age-related maculopathy. Microsc. Res. Tech. *36*, 106–122.

Latz, E., Xiao, T.S., and Stutz, A. (2013). Activation and regulation of the inflammasomes. Nat. Rev. Immunol. *13*, 397–411.

Marneros, A.G., Fan, J., Yokoyama, Y., Gerber, H.P., Ferrara, N., Crouch, R.K., and Olsen, B.R. (2005). Vascular endothelial growth factor expression in the retinal pigment epithelium is essential for choriocapillaris development and visual function. Am. J. Pathol. *167*, 1451–1459.

Martin, D.F., Maguire, M.G., Ying, G.S., Grunwald, J.E., Fine, S.L., and Jaffe, G.J.; CATT Research Group. (2011). Ranibizumab and bevacizumab for neovascular age-related macular degeneration. N. Engl. J. Med. *364*, 1897–1908.

Miquerol, L., Gertsenstein, M., Harpal, K., Rossant, J., and Nagy, A. (1999). Multiple developmental roles of VEGF suggested by a LacZ-tagged allele. Dev. Biol. *212*, 307–322.

Monaghan-Benson, E., and Burridge, K. (2009). The regulation of vascular endothelial growth factor-induced microvascular permeability requires Rac and reactive oxygen species. J. Biol. Chem. *284*, 25602–25611.

Oh, H., Takagi, H., Takagi, C., Suzuma, K., Otani, A., Ishida, K., Matsumura, M., Ogura, Y., and Honda, Y. (1999). The potential angiogenic role of macrophages in the formation of choroidal neovascular membranes. Invest. Ophthalmol. Vis. Sci. *40*, 1891–1898.

Sunness, J.S., Gonzalez-Baron, J., Bressler, N.M., Hawkins, B., and Applegate, C.A. (1999). The development of choroidal neovascularization in eyes with the geographic atrophy form of age-related macular degeneration. Ophthalmology *106*, 910–919.

Takeda, K., Tsutsui, H., Yoshimoto, T., Adachi, O., Yoshida, N., Kishimoto, T., Okamura, H., Nakanishi, K., and Akira, S. (1998). Defective NK cell activity and Th1 response in IL-18-deficient mice. Immunity *8*, 383–390.

Tarallo, V., Hirano, Y., Gelfand, B.D., Dridi, S., Kerur, N., Kim, Y., Cho, W.G., Kaneko, H., Fowler, B.J., Bogdanovich, S., et al. (2012). DICER1 loss and Alu RNA induce age-related macular degeneration via the NLRP3 inflammasome and MyD88. Cell *149*, 847–859.

Tseng, W.A., Thein, T., Kinnunen, K., Lashkari, K., Gregory, M.S., D'Amore, P.A., and Ksander, B.R. (2013). NLRP3 inflammasome activation in retinal pigment epithelial cells by lysosomal destabilization: implications for age-related macular degeneration. Invest. Ophthalmol. Vis. Sci. *54*, 110–120.

van Leeuwen, R., Klaver, C.C., Vingerling, J.R., Hofman, A., and de Jong, P.T. (2003). Epidemiology of age-related maculopathy: a review. Eur. J. Epidemiol. *18*, 845–854.

Wen, H., Gris, D., Lei, Y., Jha, S., Zhang, L., Huang, M.T., Brickey, W.J., and Ting, J.P. (2011). Fatty acid-induced NLRP3-ASC inflammasome activation interferes with insulin signaling. Nat. Immunol. *12*, 408–415.

Wen, H., Ting, J.P., and O'Neill, L.A. (2012). A role for the NLRP3 inflammasome in metabolic diseases—did Warburg miss inflammation? Nat. Immunol. *13*, 352–357.

Wilkie, A.L., Jordan, S.A., and Jackson, I.J. (2002). Neural crest progenitors of the melanocyte lineage: coat colour patterns revisited. Development *129*, 3349–3357.

Wu, K.H., Madigan, M.C., Billson, F.A., and Penfold, P.L. (2003). Differential expression of GFAP in early v late AMD: a quantitative analysis. Br. J. Ophthalmol. *87*, 1159–1166.

Yu, Y., Bhangale, T.R., Fagerness, J., Ripke, S., Thorleifsson, G., Tan, P.L., Souied, E.H., Richardson, A.J., Merriam, J.E., Buitendijk, G.H., et al. (2011). Common variants near FRK/COL10A1 and VEGFA are associated with advanced age-related macular degeneration. Hum. Mol. Genet. *20*, 3699–3709.